A Transformerless Medium-Voltage STATCOM Topology Based on Extended Modular Multilevel Converters

H. Mohammadi P., *Student Member, IEEE*, and M. Tavakoli Bina, *Senior Member, IEEE*

***Abstract*—A new transformerless four-leg topology is suggested for shunt compensation, the modular multilevel converters (MMC) based on the half-bridge converters, to achieve higher performance as a STATCOM in a distorted and unbalanced medium-voltage large-current (MV-LC) system. Further, an extended MMC (EMMC) is proposed in order to manage more accurate compensation for high-power applications. Both proposals can be controlled for various purposes such as reactive power and unbalance compensation, voltage regulation, and harmonic cancellation. Moreover, related control strategies are also suggested for both the MMC and the EMMC to ensure that the source-end three-phase currents are sinusoidal and balanced. Also, the dc-link capacitors of the half-bridge converters are regulated. One interesting application for the EMMC-based STATCOM could be the improvement in power quality and performance of the electrified railway traction power supply system. Both the MMC- and the EMMC-based STATCOM along with their proposed control strategies were simulated; further, to verify the suggestions, these proposals were also implemented on a 30-kVA modular laboratory prototype. Experiments and simulations confirm the predefined objectives.**

***Index Terms*—Harmonics, medium-voltage large-current (MV-LC), modular multilevel converters, unbalanced compensation.**

NOMENCLATURE

n	Total number of the cascaded HBM in a leg.
m	Total number of the MMC in an EMMC.
k	HBM number in a leg ($0 \leq k \leq n$).
j	MMC number in the EMMC ($0 \leq j \leq m$).
L_F	Commutating inductance.
L_C	Coupling inductance.
L_S	Total inductance of the series inductors in a leg.
C_m	DC-link capacitance of an HBM.
R_S	Source resistance.
T_S	Sampling period.
τ	Time interval between two adjacent carriers.
f_{C1}	Carrier frequency of an HBM.
f_{SC}	DSP sampling frequency of the control unit.
$i_{S(abc)}$	Three-phase source currents.
$i_{L(abc)}$	Three-phase load currents.
$i_{C(abc)\text{-ref}}$	STATCOM three-phase reference currents.
$i_{C(abc)}$	STATCOM currents.
$I_{B(abc)}$	Balancing currents.
I_C	Circulating current.
$i_{C(\alpha\beta 0)\text{-ref}}$	$\alpha\beta 0$ reference currents of STATCOM.
$i_{Mj(abc)}$	abc currents of the jth MMC in the EMMC.
$i_{H\max}$	Maximum current through the cascaded HBM.
$\Delta i_{C\max}$	Maximum output current ripple of the converter.
$i_{N(abc)}$	Measured currents of the NCP-HBCC legs.
$i_{P(abc)}$	Measured currents of the PCP-HBCC legs.
$i_{N(abc)\text{-ref}}$	Reference currents for the NCP-HBCC legs.
$i_{P(abc)\text{-ref}}$	Reference currents for the PCP-HBCC legs.
$i_{N(abc)}$	Total current of the NCP-HBCC legs in an EMMC.
$i_{P(abc)}$	Total current of the PCP-HBCC legs in an EMMC.
V_N	Voltage of the neutral point ($V_N = 0$).
$V_{S(abc)}$	Source voltages.
$V_{(abc)}$	Voltages of the PCC.
V_{Cm}	DC-link voltage of the mth HBM.
V_{CM}	Mean of all HBM's dc-link voltages.
$V_{\mathrm{CM\text{-}ref}}$	Reference voltage of V_{CM}.
$V_{\mathrm{CN}(abc),\mathrm{k}}$	Measured dc voltage of the kth HBM of the NCP.
$V_{\mathrm{CP}(abc),\mathrm{k}}$	Measured dc voltage of the kth HBM of the PCP.
V_{PCP}	Voltage between PCP and the neutral point.
V_{NCP}	Voltage between NCP and the neutral point.
V_{DCM}	Voltage between PCP and NCP (V_{PCP}-V_{NCP}).
$V_{N(abc)\text{-ref}}$	Reference voltage for the NCP-HBCC legs.
$V_{P(abc)\text{-ref}}$	Reference voltage for the PCP-HBCC legs.
V_{LN}, V_{LP}	Voltage drop on L_F of the NCP and PCP-HBCC legs.
$V_{C(abc)\text{-ref}}$	Reference voltages of the pair-legs.
$V_{(abc)1}$	Fundamental positive-sequence of the point of common coupling (PCC) voltage.
$\Delta V_{C\max}$	Maximum voltage ripples on the dc-link capacitors.
P_{Loss}	Total power losses of STATCOM.
p_{Load}	Instantaneous active power of the load.
q_{Load}	Instantaneous reactive power of the load.
$p_{N(abc)}(t)$	Instantaneous power of the NCP–HBCC legs.

Manuscript received April 19, 2010; revised July 18, 2010; accepted September 30, 2010. Date of current version June 29, 2011. Recommended for publication by Associate Editor P.-T. Tai.

The authors are with the Faculty of Electrical and Computer Engineering, K. N. Toosi University of Technology, Tehran 16315-1355, Iran (e-mail: mohammadi@kntu.ac.ir; tavakoli@kntu.ac.ir).

Color versions of one or more of the figures in this paper are available online at http://ieeexplore.ieee.org.

Digital Object Identifier 10.1109/TPEL.2010.2085088

$p_{P(abc)}(t)$	Instantaneous power of the PCP-HBCC legs.
$P_{N(abc)}$	DC component of $p_{N(abc)}(t)$.
$P_{P(abc)}$	DC component of $p_{P(abc)}(t)$.
$p_{\mathrm{NO}(abc)}(t)$	AC component of $p_{N(abc)}(t)$.
$P_{\mathrm{PO}(abc)}(t)$	AC component of $p_{P(abc)}(t)$.
$D_{(abcN)\text{-ref}}$	Reference duty cycle calculated for the pair-legs.
$D_{N(abcN)\text{-ref}}$	Duty cycle of the NCP-HBCC legs.
$D_{P(abcN)\text{-ref}}$	Duty cycle of the PCP-HBCC legs.

I. Introduction

MODERN medium-voltage distribution systems supply nonlinear loads such as single-phase ac traction systems. These loads make the network to operate under undesired conditions, i.e., distorted, uncontrolled reactive power and significant unbalance enforcement [1], [2]. Therefore, these associated inevitable issues ought to be simultaneously resolved to achieve acceptable power quality level. Meanwhile, mitigation of all these power quality problems by means of a single compensator is a challenging task in a medium-voltage network [3], [4].

A full-bridge cascaded converter (FBCC) could be directly connected to a medium-voltage network [5], [6]. However, the FBCC has been established as the most preferred solution for managing reactive power in distribution systems, improving the power quality in the medium-voltage high-power industries. Unlike diode-clamped multilevel converters (DCMC) and flying-capacitor-clamped multilevel converters (FCMC), the FBCC introduces lower total losses along with higher reliability [7], [19]. Meanwhile, they have their restrictions when operating under distorted unbalance situations in a medium-voltage network compared to those of the DCMC and the FCMC [3]–[8]. In the mean time, a three-phase FBCC, connected in delta or star type, is unable to fully compensate the source currents when the unbalanced loads containing harmonics. A delta-connected FBCC cannot generate zero sequence components flowing through the fourth neutral-wire. Also, balancing an unbalanced load using a star-connected FBCC is faced with some complications. Assume that a star-connected FBCC-based STATCOM is balancing three different active powers supplied by the source. Then, a certain average real power has to either flowing into or out of individual series connected full-bridge converters (leg). This results in either dc-link build-up or discharge of capacitors in that leg. In other words, the unbalanced currents of the star connected FBCC imposes unequal active power exchange by the FBCC legs. This makes the dc voltage balancing for the storage capacitors in all three legs much complicated [9].

The idea of modular multilevel converters (MMC) was first introduced by Marquardt for medium-voltage applications [10]. These converters consist of two similar parallel half-bridge cascaded converters (HBCC) per phase (three-phase in star-connected configuration). Due to the modularity of these converters, they are very attractive for high voltage dc transmission (HVDC), flexible ac transmission systems (FACTS), and medium-voltage drives [11], [12]. The main advantage of applying the MMC as a STATCOM [13] is that they could operate under unbalanced and distorted voltages and currents properly, while voltages of the dc-link capacitors remains balanced [9].

Hence, this paper proposes a new type of the MMC topology as a STATCOM in order to achieve full compensation of MV-LC loads, i.e., harmonic elimination, reactive power optimization and in particular balancing the three- or four-wire systems. The full compensation using the proposed STATCOM is achieved without any coupling transformer for MV-LC applications (high-power). Nevertheless, available power semiconductor technology may impose limitations due to the voltage and current ratings, losses, and switching frequency. Hence, here the EMMC is proposed that is composed of parallel connection of multiple MMC per phase in order to deal with large-current requirements. There are two main differences between the EMMC and just parallel connection of MMC: 1) two or more MMC in an EMMC share the common dc-link (positive and negative common points); and 2), the presence of the coupling inductors that lowers down considerably the circulating current between them. The EMMC produces higher quality waveforms for the network compared to the MMC, reducing the conductive electromagnetic interference concerns in large-current applications. Also, paralleling multiple MMC improves reliability, performance, and efficiency of the overall system, making it more flexible. This paper is initially focusing on description of the MMC-based STATCOM, both the proposed power circuit and control algorithms. Then, the EMMC topology is introduced, suggesting an improved modulation technique along with a control algorithm. The compensating current signals are extracted based on the instantaneous power theory, while here the introduced control algorithm in [9] is extended to present for a new real-time current control technique based on the predictive control method for both the MMC and EMMC applicable to microcontrollers like DSP. Furthermore, the modulating technique is related to the controller such that capacitor voltage balancing is working properly even under unbalanced conditions for the converter. Both original and extended topologies were simulated separately in the presence of the same network, where the simulations are compared accordingly. A 30 kVA, 400 V modular laboratory prototypes was designed and implemented, consisting of eight half-bridge modules (HBM), in order to assess the performance of both the proposed MMC and EMMC. Experimental results are presented to verify the proposed power circuit operation under the suggested control algorithms as well as the modulation technique. Finally, a comparative discussion is presented to evaluate the performance and practical capabilities of each of the two topologies.

II. MMC-Based STATCOM Proposition

The MMC-based STATCOM is composed of two parallel connected complementary HBCC as shown in Fig. 1. Each star-connected HBCC has either three or four similar legs (cascaded HBM). While one HBCC has a negative common point (NCP), the other one has a positive common point (PCP). Both the NCP and PCP are float. To compensate a three-wire distorted load, the converter can be composed of two three-leg complementary HBCC. The number of levels, in a general $(n+1)$-level MMC,

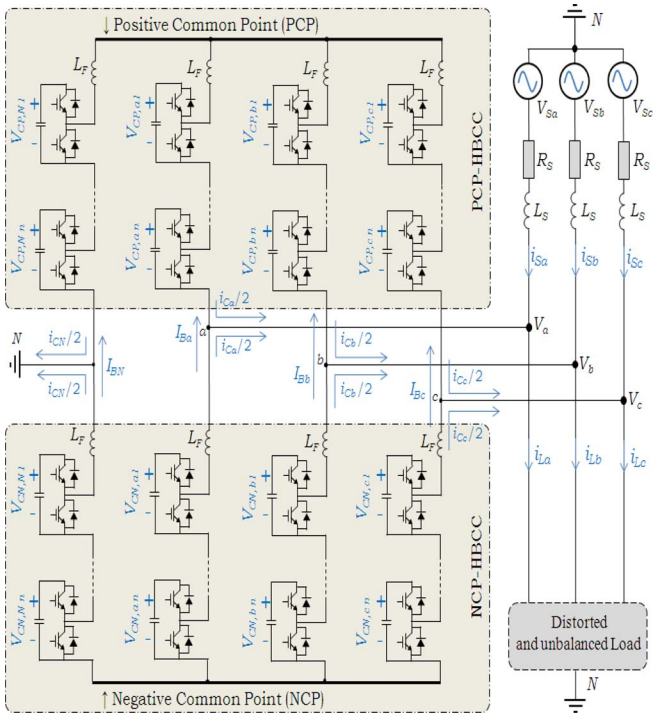

Fig. 1. Configuration of the proposed MMC-based STATCOM.

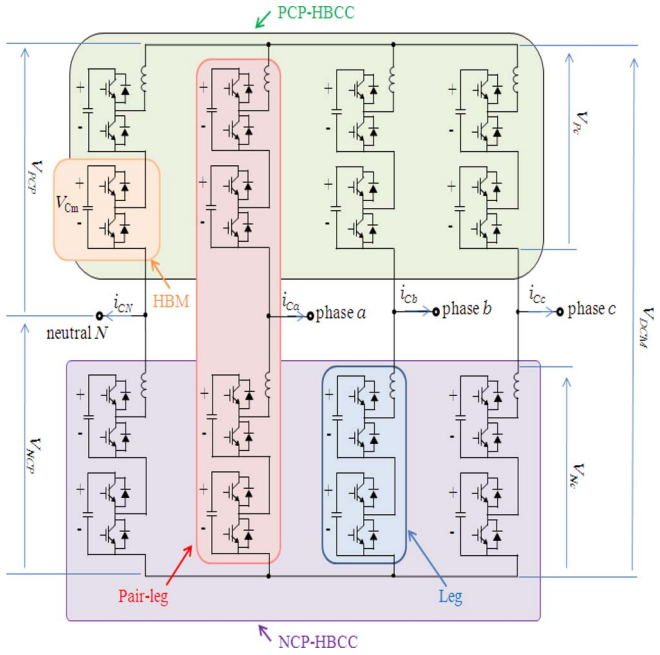

Fig. 2. Detailed description of different parts of the proposed MMC.

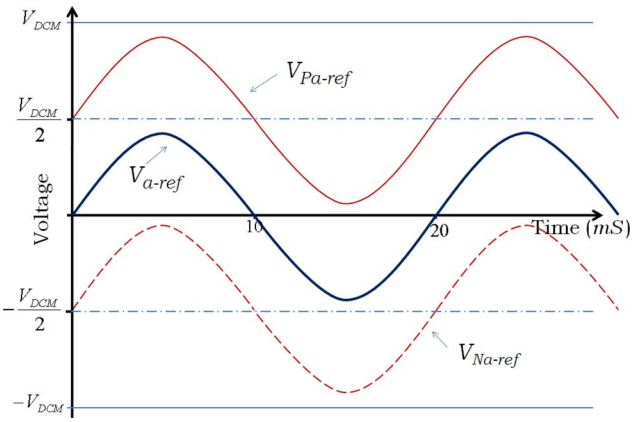

Fig. 3. Reference voltages of the NCP-HBCC and the PCP-HBCC legs against the voltage of the PCC all for phase *a*.

is defined by the available *n* identical HBM cascaded in each leg. Then, all $(n+1)$-level legs are connected to the network using an inductive filter (L_F). All HBM have the same semiconductor ratings as well as identical dc-link capacitance. Therefore, each HBM can be assumed as an identical two-terminal device. Voltage regulation of the dc-link capacitors is achieved without any additional connections or energy transfer circuits to the associated HBM.

Considering the detailed picture of the proposed MMC in Fig. 2, each HBM is capable of producing either V_{Cm} (the *m*th dc-link capacitor voltage) or zero at any given instance. Thus, the resultant voltage of *n* cascaded HBM varies within [0, $V_{\rm DCM}$], where $V_{\rm DCM} = nV_{Cm}$. Hence, all phase-to-phase voltages on each HBCC are obtained through a KVL over two identical opposite polarity legs (each leg controlled independently) by ignoring the inductor voltages (see Fig. 2). In other words, the voltage between any two phases of an HBCC can be adjusted between $+V_{\rm DCM}$ and $-V_{\rm DCM}$.

Moreover, one leg from the PCP-HBCC along with another leg from the NCP-HBCC is coupled with the same phase (see pair-leg in Fig. 2). These two legs constantly complement each other as shown in Fig. 3, averaging the pair-leg waveforms at each phase. As a result, the voltage difference between the NCP and the PCP ($V_{\rm PCP}$–$V_{\rm NCP}$) is always $V_{\rm DCM}$ (the voltage drops on L_F is negligible). Thus, the voltage between the PCP and the neutral point *N* is $V_{\rm DCM}/2$, and the voltage between NCP and *N* is $-V_{\rm DCM}/2$. Although the voltage across a leg has a dc component, there exists no dc component on any phase-to-phase voltage of an HBCC. To enable compensation of inductive loads, the value of $V_{\rm DCM}$ must be chosen greater than peak-to-peak amplitude of the line voltage [14]. It should be noticed that both legs of a pair-leg are controlled such that supplying constantly one half of the total current per phase for the MMC.

A. Definition of Balancing Current

When the MMC provides unbalanced currents to compensate the nonlinear unbalanced load, one output phase of the MMC may produce active power while the other phases consume active power. This causes discharge of those capacitors supplying active power, and charge of those capacitors consuming active power. Since each leg of a pair-leg supplies half of a phase current, the capacitor voltages of each pair-leg share equal changes. Meanwhile, unequal capacitor voltages of two pair-legs, connected to two different phases, cause a direct balancing current (I_B) flowing from the overcharged pair-leg toward the undercharged pair-leg [15]. Under such circumstances, the total current of each leg of the NCP-HBCC and the PCP-HBCC is

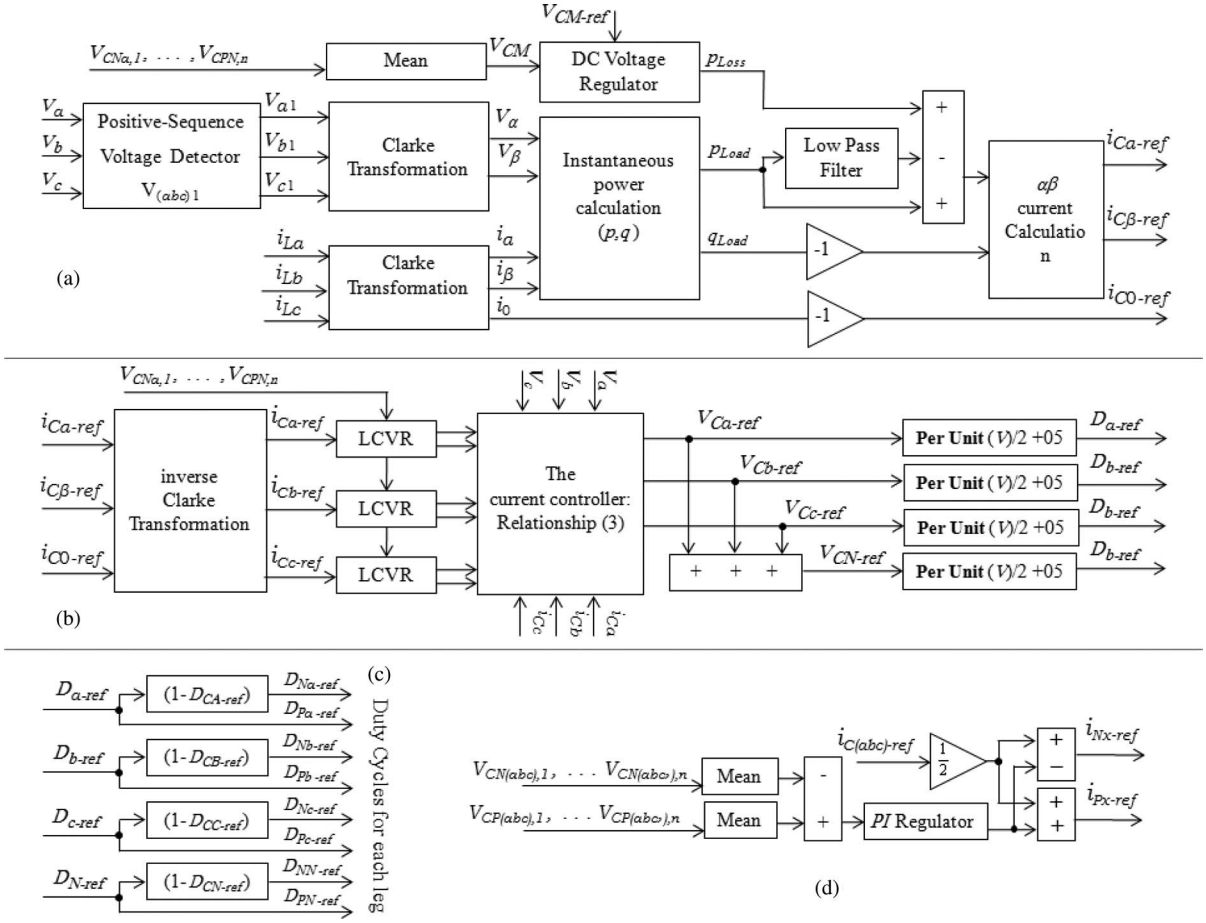

Fig. 4. Controller unit for both the MMC and the EMMC-based STATCOM, (a) derivation of the three-phase reference currents, (b) current controller diagram, (c) duty cycle extraction to generate switching modulation, and (d) local capacitor voltage regulator for both legs connected to one terminal (pair-leg).

equal to $(x = a, b, c, N)$

$$\begin{bmatrix} i_{Nx} \\ i_{Px} \end{bmatrix} = \begin{bmatrix} \dfrac{i_{Cx}}{2} + I_{Bx} \\ \dfrac{i_{Cx}}{2} - I_{Bx} \end{bmatrix} \tag{1}$$

where i_{Nx}, i_{Px}, and i_{Cx} are the NCP-HBCC, PCP-HBCC, and STATCOM currents, respectively. The balancing current magnitude in each pair-leg (I_{Bx}) depends on the value of active power interchanged between the network and the pair-leg. The presence of this balancing current makes the stored energy at all legs to remain balanced. At the same time, any balancing current fluctuations are attenuated through the inductance L_F.

B. Control Methodology

Assume that the controller unit in the MMC-based device is performing a full compensation as a STATCOM. Hence, the following tasks can be discussed.

1) Proper Reference Currents for STATCOM: The general instantaneous power theory [16] was used to derive the reference currents for each output phase of the MMC-based STATCOM as described in Fig. 4(a). The objective of this compensation theory is to make the source currents completely sinusoidal and balanced; i.e., in phase with the fundamental positive sequence component of the source voltage.

2) Calculation of the Reference Voltage for Each Leg: Having calculated the three-phase reference currents of the MMC- or EMMC-based STATCOM, if V_{LNx} and V_{LPx} are the NCP-HBCC and PCP-HBCC voltage drops on L_F (the commutating inductance), then the three-phase reference voltages of STATCOM can be worked out as follows $(x = a, b, c)$ [see Fig. 4(b)]:

$$\begin{aligned} \begin{bmatrix} V_{Nx\text{-ref}} \\ V_{Px\text{-ref}} \end{bmatrix} &= \begin{bmatrix} V_x - V_{LNx} - V_{\text{NCP}} \\ V_x - V_{LPx} - V_{\text{PCC}} \end{bmatrix} \\ &= \begin{bmatrix} V_x - L_F \dfrac{d(i_{Cx} + 2I_{Bx})}{2dt} + \dfrac{V_{\text{DCM}}}{2} \\ V_x - L_F \dfrac{d(i_{Cx} - 2I_{Bx})}{2dt} - \dfrac{V_{\text{DCM}}}{2} \end{bmatrix} \\ &= \begin{bmatrix} V_x - L_F \dfrac{d(i_{Cx})}{2dt} + \dfrac{V_{\text{DCM}}}{2} \\ V_x - L_F \dfrac{d(i_{Cx})}{2dt} - \dfrac{V_{\text{DCM}}}{2} \end{bmatrix}. \end{aligned} \tag{2}$$

Assume that the derivation of I_{Bx} is ignored in (2) for the steady-state operation of STATCOM. By neglecting the resistance associated with L_F, (2) can be employed as a current controller for STATCOM to track the reference currents. To implement the current controller with a DSP, (2) can be represented in a discrete form with a good approximation as

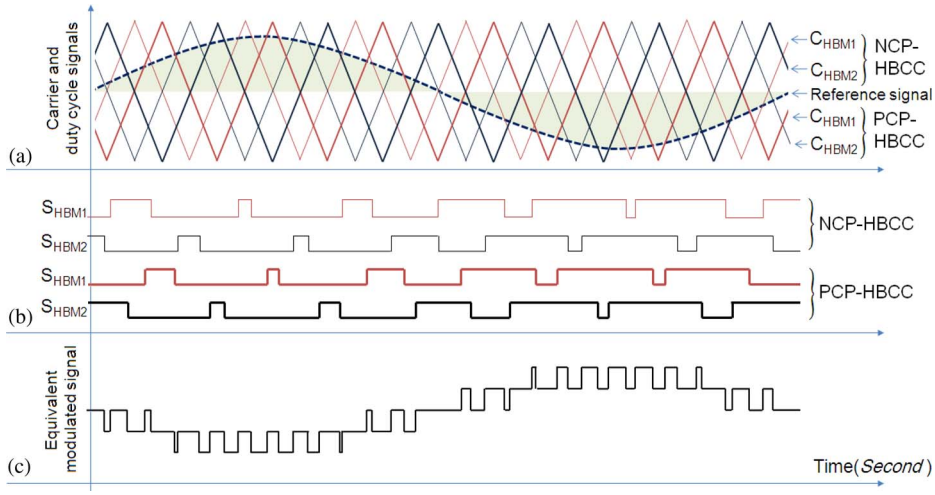

Fig. 5. Phase-shifted PWM modulation technique to create switching signals for four HBM of the MMC having two HBM per leg: (a) carrier signals of the NCP-HBCC and the 180° phase shifted PCP-HBCC, (b) switching pattern generated for four HBM of the pair-leg, and (c) equivalent modulated signal.

follows:

$$\begin{bmatrix} V_{Nx\text{-ref}}(z) \\ V_{Px\text{-ref}}(z) \end{bmatrix} = \begin{bmatrix} V_x(z-1) - \dfrac{L_F(i_{Cx\text{-ref}}(z) - i_{Cx}(z-1))f_{\text{sc}}}{2} + \dfrac{V_{\text{DCM}}}{2} \\ V_x(z-1) - \dfrac{L_F(i_{Cx\text{-ref}}(z) - i_{Cx}(z-1))f_{\text{sc}}}{2} - \dfrac{V_{\text{DCM}}}{2} \end{bmatrix} \tag{3}$$

where x stands for a, b, or c, $i_{Cx\text{-ref}}$ denotes the STATCOM reference current in the phase x, $V_{Nx\text{-ref}}$ and $V_{Px\text{-ref}}$ are the predicted reference voltage for the NCP–HBCC-leg and the NCP–HBCC-leg in the phase x, respectively, and f_{SC} is the DSP sampling frequency of the control unit. The voltage $V_{Cx\text{-ref}}$ in Fig. 4 can be obtained from (3) when both sides of (3) are normalized by $V_{\text{DCM}}/2$ as (4) shown at the bottom of the page, where $D_{Nx\text{-ref}}$ and $D_{Px\text{-ref}}$ are the duty cycles of NCP–HBCC and PCP–HBCC legs, respectively, and $V_{Cx\text{-ref}}$ is the predicted reference value of the pair-leg for the phase x.

3) Switching Modulation for Each HBM: A phase-shifted PWM modulation technique is introduced in [18] and [20] for the cascaded HBM. The main goal is to share linearly the load among all HBM. Therefore, as shown in Fig. 5, each HBM has an independent carrier signal, while the reference signal is shared by all the series HBM in each leg. The switching instants of each HBM are generated by the comparison of the leg reference voltage and the HBM carrier signal. To reduce the output current ripple of the MMC, the carrier signals for the NCP–HBCC are shifted by 180° compared to those of the PCP-HBCC correspondingly (see Fig 5). Therefore, the output current ripple of the MMC can reciprocally be canceled up to 50% in comparison with the ripples of the HBCC.

4) Capacitor Voltage Balancing of all HBM: Each HBM has two complementary switches in series, providing either the dc-link voltage or zero for the output. When this output voltage of the HBM is set to its dc-link voltage, a positive input current ($i_{Nx} > 0$) decreases the capacitor voltages of the NCP–HBCC, and increases those of the PCP–HBCC. Similarly, a negative input current ($i_{Nx} < 0$) increases the capacitor voltages of the NCP–HBCC, and decreases those of the PCP–HBCC. Otherwise, when the output voltage of the HBM is zero, the capacitor voltage will not change. These switching effects can be used for capacitor voltage balancing. Thus, for balanced load sharing of all HBM in a leg, the measured capacitor voltages of the leg are sorted in ascending order for each switching period. The sign of the leg current and the number of HBM that are permanently set to its dc-link voltage determine that HBM should be selected [12]. In fact, the explained algorithm is a combination of PS–PWM with a procedure that selects those HBM need to be activated among all HBM available in a leg.

Instantaneous power of a pair-leg ($p_{Nx}(t)$ and $p_{Px}(t)$) can be calculated using (1) and (3), having a dc component (P_{Nx} and P_{Px}) along with an alternative component ($p_{NOx}(t)$ and

$$\begin{cases} \begin{bmatrix} V_{Nx\text{-ref}}(z) \\ V_{Px\text{-ref}}(z) \end{bmatrix}_{\text{Normalized}} = \begin{bmatrix} D_{Nx\text{-ref}}(z) \\ D_{Px\text{-ref}}(z) \end{bmatrix} = \begin{bmatrix} \dfrac{2V_x(z-1)}{V_{\text{DCM}}} - \dfrac{L_F(i_{Cx\text{-ref}}(z) - i_{Cx}(z-1))f_{\text{sc}}}{V_{\text{DCM}}} + 1 \\ \dfrac{2V_x(z-1)}{V_{\text{DCM}}} - \dfrac{L_F(i_{Cx\text{-ref}}(z) - i_{Cx}(z-1))f_{\text{sc}}}{V_{\text{DCM}}} - 1 \end{bmatrix} = \begin{bmatrix} V_{Cx\text{-ref}}(z) + 1 \\ V_{Cx\text{-ref}}(z) - 1 \end{bmatrix} \\ V_{Cx\text{-ref}}(z) = \dfrac{2V_x(z-1)}{V_{\text{DCM}}} - \dfrac{L_F(i_{Cx\text{-ref}}(z) - i_{Cx}(z-1))f_{\text{sc}}}{V_{\text{DCM}}} \end{cases} \tag{4}$$

$p_{POx}(t)$) for each leg as follows ($x = a, b,$ or c):

$$\begin{bmatrix} p_{Nx}(t) \\ p_{Px}(t) \end{bmatrix} = \begin{bmatrix} P_{Nx} \\ P_{Px} \end{bmatrix} + \begin{bmatrix} p_{NOx}(t) \\ p_{POx}(t) \end{bmatrix}. \tag{5}$$

The dc term (nonzero average value over 50/60 Hz) is equal to

$$\begin{bmatrix} P_{Nx} \\ P_{Px} \end{bmatrix} = \begin{bmatrix} \frac{i_{Cx}V_x}{2} - \frac{i_{Cx}L_F(i_{Cx\text{-ref}} - i_{Cx})f_{sc}}{4} + \frac{I_{Bx}V_{\mathrm{DCM}}}{2} \\ \frac{i_{Cx}V_x}{2} - \frac{i_{Cx}L_F(i_{Cx\text{-ref}} - i_{Cx})f_{sc}}{4} + \frac{I_{Bx}V_{\mathrm{DCM}}}{2} \end{bmatrix} \tag{6}$$

and the ac term (zero average value over 50/60 Hz) is equal to

$$\begin{bmatrix} p_{NOx}(t) \\ p_{POx}(t) \end{bmatrix} = \begin{bmatrix} I_{Bx}V_x - \frac{I_{Bx}L_F(i_{Cx\text{-ref}} - i_{Cx})f_{\mathrm{sc}}}{2} + \frac{i_{Cx}V_{\mathrm{DCM}}}{4} \\ -I_{Bx}.V_x + \frac{I_{Bx}L_F(i_{Cx\text{-ref}} - i_{Cx})f_{\mathrm{sc}}}{2} - \frac{i_{Cx}V_{\mathrm{DCM}}}{4} \end{bmatrix}. \tag{7}$$

Since both components in (6) are similar, the average active power is the same at 50/60 Hz for both legs of a pair-leg. Therefore, variations of the capacitor voltages for a pair-leg are the same too.

Due to nonideal nature of the converter elements, there is a slight difference between the capacitor voltages of the two legs of a pair-leg. This may be corrected by using appropriate local controller to adjust current contribution for the two legs as shown in Fig. 4(d). There are four local capacitor voltage regulators in the MMC that each regulates the capacitor voltages of a pair-leg. This technique assures balance of the capacitor voltages for all HBM in the converter. To regulate the dc voltage of all capacitors at a predetermined reference value, a dc voltage regulator unit is added in the reference current controller unit. The mean value of all capacitor voltages is regulated toward a certain value by estimating power losses through a dc voltage regulator unit, adding it to the reference output power of the converter as shown in Fig. 4(a).

III. EMMC-Based STATCOM

Here the EMMC-based STATCOM is proposed for full compensation of the MV-LC loads such as electric traction systems. The suggested high power STATCOM comprises of two or more identical MMC all connected in parallel. A simple model of the EMMC-based STATCOM, having two MMC, is shown in Fig. 6. While all MMC have the same electrical specification, all NCP legs connected together, and the same is done for all PCP legs to achieve a better voltage regulation for the capacitors. Hence, voltage regulation for the HBM capacitors is managed without any additional connections or energy transfer circuits.

The total output current of each phase is equally supplied by all legs coupled to that phase. For instance, each HBCC of the

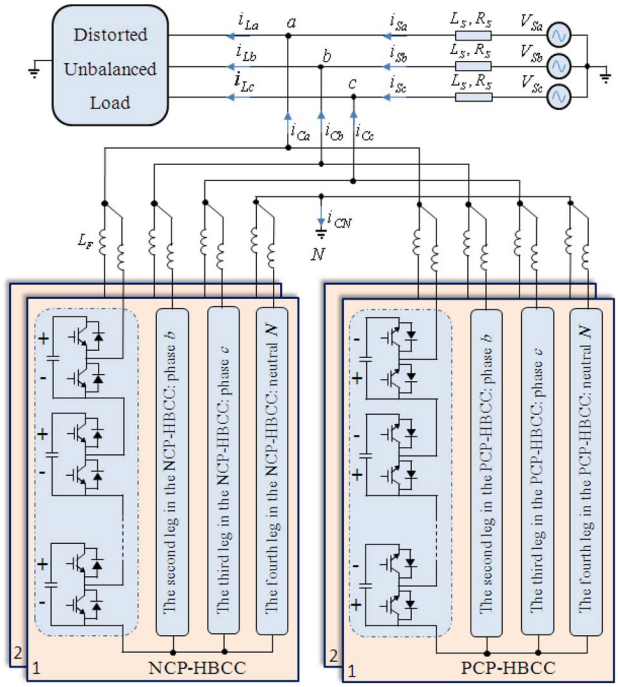

Fig. 6. Structure of the EMMC that is composed of two parallel MMC, connected to the network.

STATCOM, shown in Fig. 6, provides a quarter of the output current for each phase. Subsequently, for *m* parallel MMC, the nominal current rating for all HBM is specified by

$$i_{H\max} = \left.\frac{\max(i_x)}{2m}\right|_{x=a,b,c,N} \tag{8}$$

where max (i_x) is the maximum output current coming out of STATCOM. The balancing current magnitude for each leg depends on the share of active power flowing into or out of that leg. It can be seen from the circuit structure (see Fig. 6) that the sum of balancing current for each HBCC is zero, namely

$$I_{\mathrm{Ba}} + I_{\mathrm{Bb}} + I_{\mathrm{Bc}} + I_{\mathrm{BN}} = 0. \tag{9}$$

Therefore, considering (5) and (9), the stored energy of all legs remains balanced, a necessary condition for the capacitor voltage balancing purposes.

A. Switching Modulation of the EMMC

Considering the discussed current sharing for the EMMC-based STATCOM, (3) has to be rewritten in order to calculate the instantaneous reference voltages for each leg (V_{Nx} and V_{Px}) of the EMMC-based STATCOM containing *m* parallel MMC as follows:

$$\begin{bmatrix} V_{Nx\text{-ref}} \\ V_{Px\text{-ref}} \end{bmatrix} = \begin{bmatrix} V_x - \frac{L_F(i_{Cx\text{-ref}} - mi_{Cx})f_{sc}}{2m} + \frac{V_{\mathrm{DCM}}}{2} \\ V_x - \frac{L_F(i_{Cx\text{-ref}} - mi_{Cx})f_{sc}}{2m} - \frac{V_{\mathrm{DCM}}}{2} \end{bmatrix}. \tag{10}$$

The reference voltages obtained by (10) is identical for all corresponding legs of each MMC within the EMMC. A phase-shift PWM modulation technique, similar to that of the

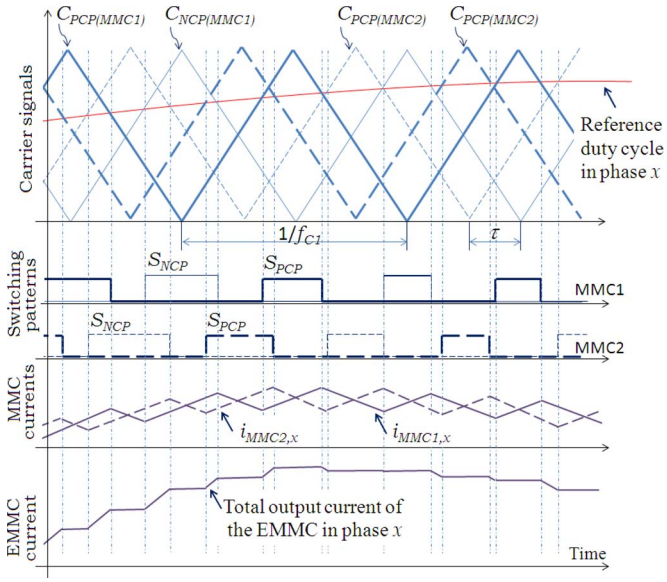

Fig. 7. Illustration of the EMMC switching pattern modulation based on the phase-shift PWM, assuming the EMMC includes two MMC (their carriers are shifted by 180° to reduce the ripple of output current) and one HBM per leg.

MMC-based STATCOM, can be applied to the EMMC. Therefore, the switching pattern for each HBM is obtained by comparing the general reference voltage with the carrier signal of each HBM as shown in Fig. 7. Carrier signals used for all shunted MMC are relatively shifted to each other to lower the output current ripple of STATCOM as follows:

$$\tau = \frac{1}{f_{C1} nm} \tag{11}$$

where τ is the time interval between two adjacent carrier signals, f_{C1} is the carrier frequency, n is the number of HBM in each leg, and m is the number of MMC in the EMMC.

B. Circulating Currents

The inductance L_F in series with each leg can substantially lower down fluctuation of the output currents. The switching signals for each HBM, in a pair-leg, are generated by different triangular carrier signals as shown in Fig. 7. Hence, because of asynchronous switching signals in those legs, the presence of a circulating current between parallel MMC (I_C) would be unavoidable. The bigger the inductance L_F, the lower will be this circulating current amplitude. However, increasing L_F causes some drawbacks: decreases the controller efficiency, affects the frequency response, raises the inductor size, and increases the power losses.

A solution is suggested here by inserting a coupling inductor L_C in series with L_F as illustrated in Fig. 8. Considering the polarity marks, L_C shows a zero inductance in conducting common mode, being activated in differential mode. In fact, the core magnetic flux of L_C is virtually zero when all pair-legs connected to one phase share identical currents. Hence, the total series inductance remains almost unchanged. Practically, there is an insignificant inductance due to the leakage of imperfect magnetic coupling that is negligible. Further, the small circulating current in those pair-legs is lowered by the coupling inductors effectively. It should be noted that L_C has no effect on the balancing dc current I_B in steady-state operation; nonetheless, this can saturate the core. Therefore, this should be considered in the filter design procedure [17].

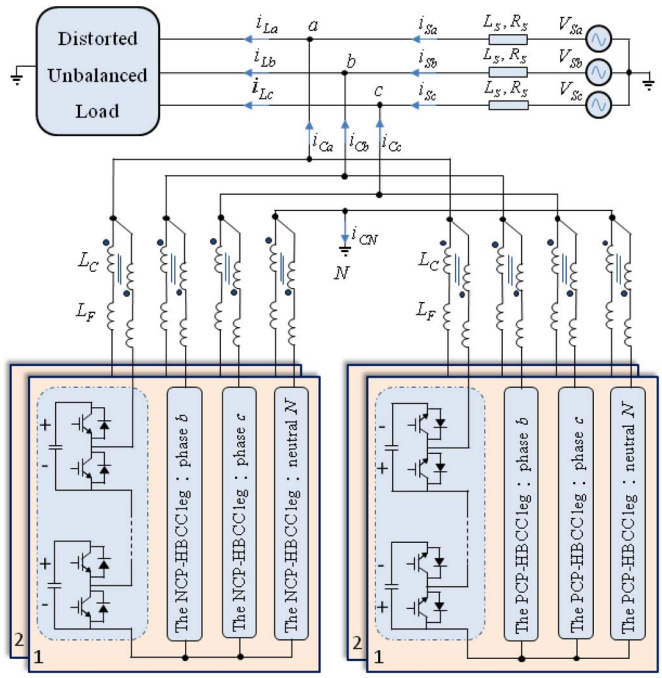

Fig. 8. Adding the coupling inductors (L_C) in series with the filter inductors (L_F) to reduce of the circulating current (I_C).

IV. Simulations and Experimental Verification

The power circuit of both MMC- and EMMC-based STATCOM proposals was simulated, where a modular laboratory prototype was also implemented for experimental confirmation.

A. Simulations

Simulations were carried out using PSIM, while the control algorithm was managed with MATLAB; then, they were linked together using SIMCOUPLER of the PSIM. Assume that a 25-kV network is supplying a distorted unbalanced load in an electrical railway application. The load is coupled across two phases of the PCC. Spectral of the load current, shown in Fig. 9, introduces a total harmonic distortion (THD) of 18.27%. Separate simulations were arranged for both the MMC and the EMMC-based STATCOM for a power rating of ±15 MVA. Each leg of the two compensators has 22 cascaded HBM. All HBM have a dc-link capacitor with a nominal dc voltage of 3.3 kV. The minimum dc-link capacitance of each HBM is determined based on the maximum allowable ripples on top of the dc voltage as follows:

$$C_m = \frac{i_{H,\max}}{f_{C1} \Delta V_{C,\max}} \tag{12}$$

where $\Delta V_{C,\max}$ is the maximum allowable voltage ripple on the

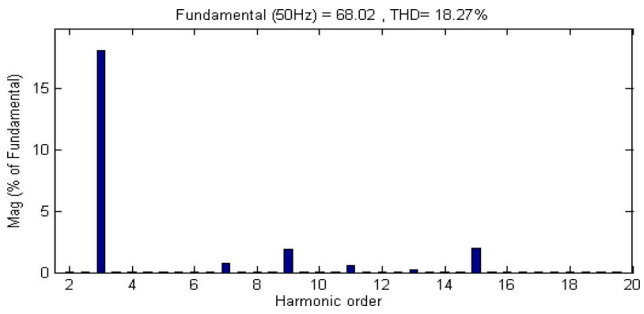

Fig. 9. Harmonic content of the simulated load current.

TABLE I
SPECIFICATIONS AND PARAMETERS USED FOR SIMULATIONS

Parameters	Symbol	Rating	
		The MMC	The EMMC
Converter power capacity	S	5 MVA	5 MVA
PCC rms line-to-line voltage	V_{LL}	25 kV	25 kV
Source inductance	L_S	200 μH (0.05%)	200 μH (0.05%)
Source resistance	R_S	25 mΩ (0.02%)	25 mΩ (0.02%)
Power system frequency	f_S	50 Hz	50 Hz
Number of HBM in each leg	n	22	22
Number of the MMC	m	1	2
Inductance of filter inductor	L_F	5 mH (1.25%)	3 mH (0.75%)
Inductance of coupling inductor	L_C	-	300 μH (0.075%)
DC-Link voltage of each HBM	V_{Cm}	3.3 kV	3.3 kV
DC-Link capacitance of each HBM	C	2.35 mF	1.1 mF
Carrier frequency	f_{C1}	1000 Hz	1000 Hz
HBM rms current rating	$i_{H\max}$	25 A	12.5 A
Normalized values are based on a 50 Hz three-phase 25kV, 5MVA			

dc-link voltages and f_{C1} is the basic carrier frequency. Since the current controller momentarily adjusts the output current of STATCOM, variation of the dc-link voltages in the allowable region will not disrupt the compensator operation. For the EMMC-based STATCOM, having two MMC, L_F and L_C contribute to the attenuation of a sudden rise of the balancing current I_{Bx} and the circulating current I_C due to an abrupt change in the load currents. Since the total series inductance L_S is almost identical for both the EMMC and the MMC, L_S is calculated according to the maximum allowable ripple on the output currents $\Delta i_{C,\max}$ as below

$$L_S = L_F + L_C = \frac{V_{\rm DCM}}{mn}\frac{T_S}{\Delta i_{C,\max}} = \frac{V_{\rm DCM}}{mnf_{C1}\Delta i_{C,\max}}. \tag{13}$$

Here, the PS–PWM modulation technique is applied to both compensators with a switching frequency of $f_{C1} = 1000$ Hz. Table I summarizes the parameters that are used in simulations.

Fig. 10 shows the simulated references of a pair-leg coupled with phase a, neglecting the series inductor voltage drop. Simulations are shown in Fig. 11, where Fig. 11(a)–(f) illustrates the PCC voltages, load currents, the EMMC currents, the source-end currents after compensation with the EMMC-based STATCOM, the MMC currents and the source-end currents after compensation with the MMC-based STATCOM, respectively. It can be seen from Fig. 11(d) and (f) that while both MMC and EMMC balance the source-end currents, the EMMC-based STATCOM produce much smoother currents than those of the MMC. Additionally, the source-end currents are in phase with the fundamentals of positive sequence voltages, containing no reactive components. Since each leg has 22 HBM, the equivalent

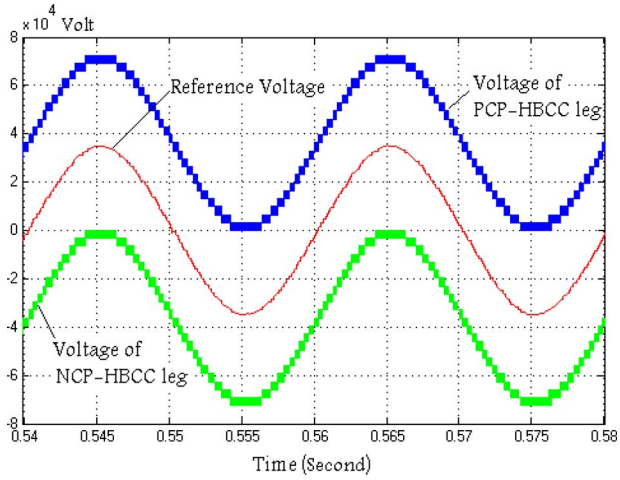

Fig. 10. Voltage of the pair-leg coupled with phase a.

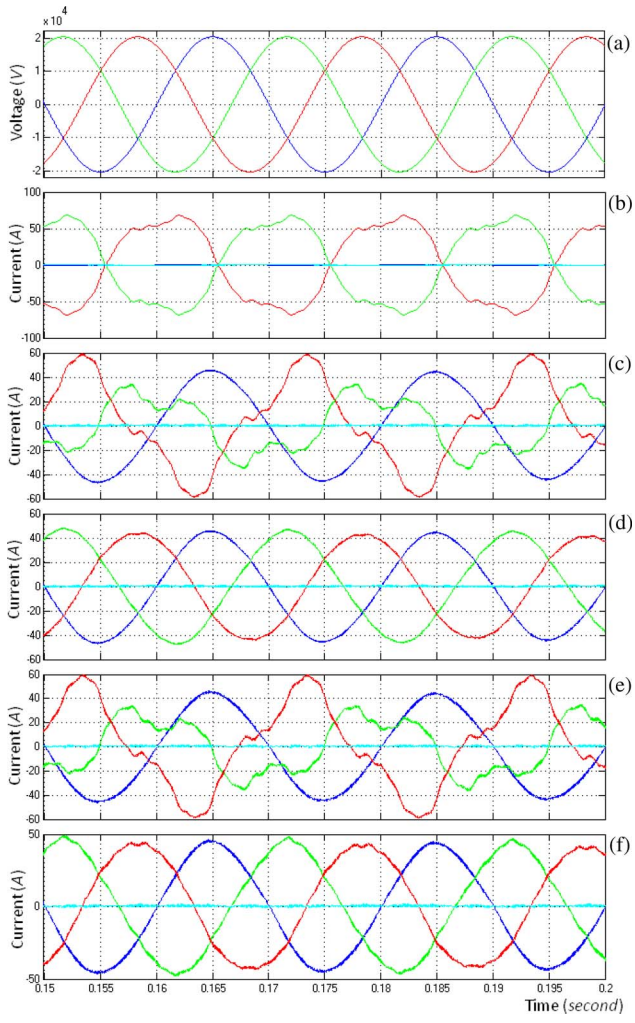

Fig. 11. Voltage and current waveforms: (a) voltages of the PCC, (b) load currents, (c) EMMC currents, (d) source-end currents after compensation by the EMMC-based STATCOM, (e) MMC currents, and (f) source-end currents after compensation by the MMC-based STATCOM.

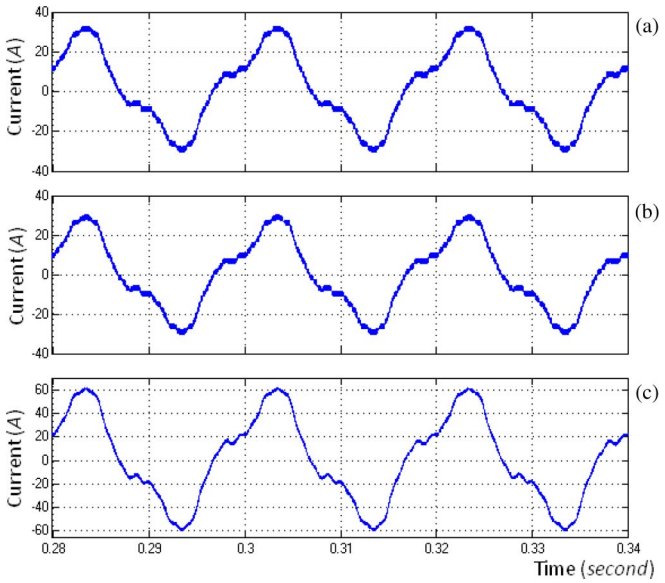

Fig. 12. Reduction of the ripple on the output current of the EMMC: (a) and (b) currents of the two parallel MMC, and (c) the resultant output current of the EMMC.

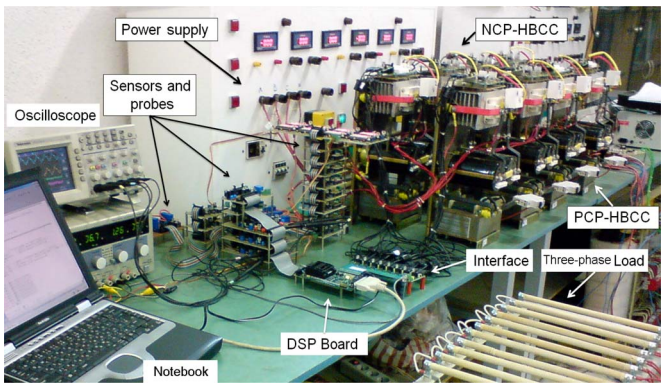

Fig. 13. The laboratory test setup where both the proposed MMC and EMMC-based STATCOM topologies were developed.

switching frequency, considering output current ripple in (13), could be up to 22 kHz for the MMC and 44 kHz for the EMMC. This implies that the output current ripples of the EMMC could be halved for both MMC as shown in Fig. 12.

B. Experimental Verification

A modular laboratory prototype was implemented in which a number of HBM, connecting inductances (L_F) and coupling inductance (L_C) can be arranged in order to obtain the desirable topology. Fig. 13 demonstrates the implemented hardware setup for the experimental work.

1) Power Circuit: The ratings of the MMC- and the EMMC-based STATCOM are shown in Table II, describing the specifications of the power system, the compensator as well as the unbalanced load. The power supply provides three-phase voltages in series with the source impedance as listed in Table II. While the source internal voltages are *distorted* (including low-order harmonics), variations on the load-terminal voltages depend on the source-end currents. Two similar MMC were arranged to demonstrate the performance of the MMC and the EMMC-based STATCOM. Each MMC consists of two four-leg star-connected HBCC; one NCP-HBCC and another one PCP-HBCC. Each leg includes one HBM that is suitable for the laboratory voltage (220 V for each phase with respect to the neutral). It should be noted that the number of HBM in each leg is determined based on the ratings of the power switches and the PCC nominal voltage.

TABLE II
SPECIFICATIONS AND PARAMETERS OF THE IMPLEMENTED MMC AND EMMC

DESCRIPTION OF PARAMETERS	RATINGS	
	THE MMC	THE EMMC
Apparent power	15 kVA	30 kVA
PCC RMS voltage	380 V	380 V
Source inductance and resistance	168 μH and 25 mΩ	168 μH and 25 mΩ
Delta-connected load impedance	*ab*: 20 Ω, *bc*: 0, *ca*: 0	*ab*: 20 Ω, *bc*: 0, *ca*: 0
Power system frequency	50 Hz	50 Hz
n	1	1
m	–	2
L_s and R_s	5 mH and 325 mΩ	5 mH and 325 mΩ
DC-link voltage of an HBM	650 V	650 V
DC-link capacitance of an HBM	2.35 mF ±10%	2.35 mF ±10%
Carrier frequency	5 kHz	5 kHz
Switches	IGBT, SKM 50GB12V	IGBT, SKM 50GB12V
i_{tmax}	25 A	25 A

2) Control Unit: Control strategies were uploaded on a DSP TMS320F2812. The control unit facilitates the communication of the DSP with the MMC and the EMMC using different parts; first, current and voltage sensor boards that measure all dc capacitor voltages, network ac voltages at the PCC, the load and the converter currents using the ADC channels of the DSP with the built-in dual sample-end hold along with analog inputs. Second, an interfacing board prepares the measured signals for the DSP analog inputs. Third, an expansion board was designed to connect the commercial evaluation board for TMS320F2812 (F2812ezDSP) to the other boards. Fourth, one board was made to redistribute and isolate the gating signals, converting the DSP outcomes (within [0, 3.3] V) into the range of [0, 15] V that is suitable for the SKPC22 boards. Fifth, the commercial SKPC 22 boards that prepares signals for the SKHI 22B IGBT driver. It is noticeable that the uploaded capacitor voltage balancing procedure, explained in Section III-B4, is general and can be applied to any number of HBM per leg.

3) Experiments (The MMC-Based STATCOM): Implementing a laboratory prototype of the compensated power system using the MMC-based STATCOM of Fig. 1, Fig. 14(a)–(b) shows the waveforms of the distorted voltages supplied by the source and unbalanced currents of the load, respectively. The source voltages contain harmonics, affecting the harmonics of the resistive load currents too. Current waveforms of the MMC-based STATCOM are shown in Fig. 14(c). To make the source-end currents balanced, the proposed compensator exchanges active power between phases; hence, the converter currents are unbalanced. A typical phase-to-phase voltage from the NCP-HBCC is shown in Fig. 14(d) (neglecting the voltage drop on L_F). The resultant source-end currents after compensation are shown in Fig. 14(e), which became balanced and in phase with the source

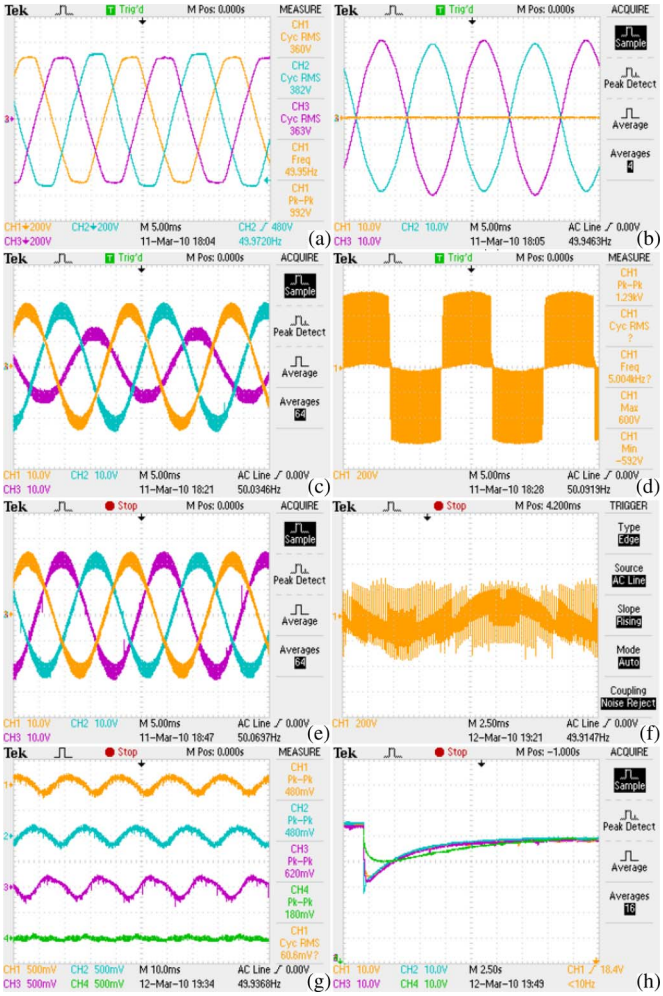

Fig. 14. Full compensation experiments with the MMC-based STATCOM: (a) three-phase distorted voltages supplied by the source, (b) three-phase unbalanced resistive load currents, (c) MMC-based STATCOM compensating currents, (d) phase-to-phase voltage drop through the NCP-HBCC (V_{Na}–V_{Nb}), (e) source-end currents after load compensation using the MMC-based STATCOM, (f) voltage drop on L_F (V_{LNa}), (g) dc-link voltage ripples of one HBCC, and (h) regulation of the dc-link voltages after connecting the load.

voltages. Moreover, a typical voltage drop on the commutating inductor (L_F) is depicted in Fig. 14(f).

Also, Fig. 14(g) provides the dc-link voltage variations for all the four HBM available in the NCP–HBCC. Finally, Fig. 14(h) illustrates how the dc-link voltage balancing performs after connecting the load to the source. While the output currents of the MMC are unbalanced, all dc-link voltages get almost converged to a predetermined reference value following a short transient. The dc-link voltage regulation is done regardless of the unbalanced output currents of the MMC. Nonetheless, the source currents introduce undesirable switching ripple contents yet.

4) Experiments: The EMMC-Based STATCOM: Next, an EMMC-based STATCOM was prepared with two MMC in parallel (MMC1 and MMC2) through the coupling inductors L_C (see Fig. 8). The distorted source and unbalanced load were identical to those of the MMC experiment. Fig. 15(a) shows output current waveforms of MMC1, MMC2, and the resultant EMMC current injected to phase a. It can be seen that the EMMC

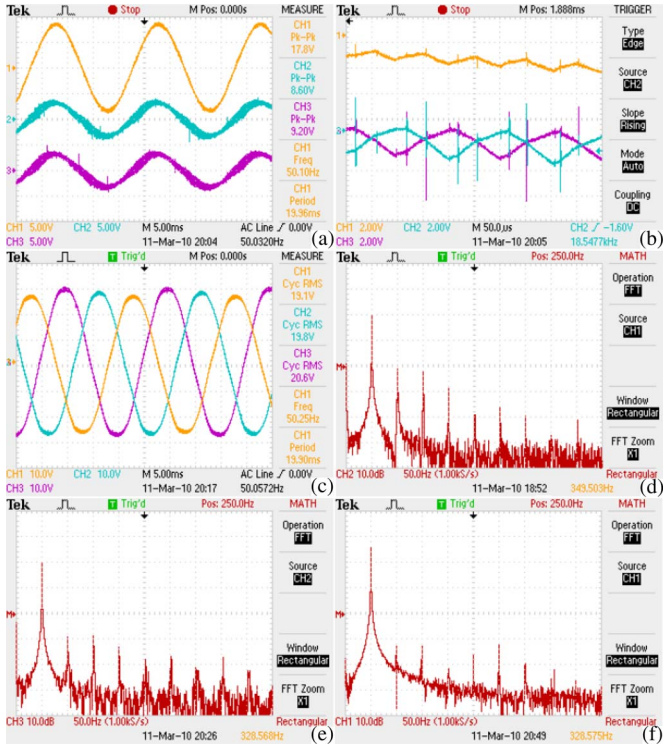

Fig. 15. Full compensation experiments with the EMMC-based STATCOM: (a) currents of the MMC1, MMC2, and EMMC (phase a), (b) ripples on currents of the MMC1, MMC2, and EMMC (phase a), (c) source-end currents after compensation with the EMMC-based STATCOM, and (d)–(f) FFT for the current of the MMC1, MMC2, and the source-end current after compensation, respectively.

current produces smoother waveform compared to those of the MMC1 and MMC2. The reason is that the carrier signals used for MMC1 are shifted by 180° for the MMC2 in order to get the lowest possible ripple for the EMMC current. Variations of the waveforms in Fig. 15(a) are zoomed out in Fig. 15(b). This is led to the ripple reduction on the source current. Fig. 15(c) illustrates the three-phase source-end currents after compensating with the EMMC-based STATCOM. Compared to the MMC, the EMMC presents better output current quality. The spectral of the three current waveforms in phase a [see Fig. 15(a)] are illustrated in Fig. 15(d)–(f) for the MMC1, the MMC2 and the source-end current after compensation with the EMMC-based STATCOM, respectively.

V. Discussion

To assess the experiments, Table III compares the THD of the monitored source currents along with the total power losses of both the MMC and EMMC-based STATCOM. It can be seen from Table III that the THD of the source currents for the EMMC are much lower than those of the MMC. While the modulating frequency is 5 kHz for one MMC, it is equivalently doubled for the EMMC with two MMC; the total power losses of the EMMC, however, remain nearly at the same level like those of the MMC. It is noticeable that a 10 kVA MMC working at 10 kHz switching frequency would introduce much higher

TABLE III
COMPARING EXPERIMENTAL LABORATORY TEST DATA BETWEEN THE MMC AND EMMC-BASED STATCOM

Parameters	The MMC	The EMMC
Tested apparent power	10 kVA	10 kVA
The THD of the source current (phase *a*)	10.18%	3.11%
The THD of the source current (phase *b*)	10.13%	3.01%
The THD of the source current (phase *c*)	10.32%	3.09%
Total power losses	493.05W (4.89%)	517.25W (5.13%)
Equvalant switching frequency	5KHz	10KHz

power losses compared to a similar EMMC-based STATCOM (10 kVA, 10 kHz).

Considering the performed simulations and experiments, although the MMC-based STATCOM is capable of full compensation, the EMMC-based STATCOM presents the following additional advantages:

1) Providing smoother output currents, smaller power losses, and improving the harmonic performance.
2) Generating higher reactive power rating with lower dc-link voltages; this implies lower voltage rating for the dc capacitor and lower stress on the switches.
3) Operating with a smaller switching frequency, resulting in smaller switching losses.
4) Increasing the reliability of the compensator even if one MMC is out of order.

Therefore, the EMMC presents higher energy efficiency, lower heat dissipation, lower weight and volume for the compensator. In fact, the EMMC has lower maintenance costs compared to the MMC. In the mean time, the high-power load compensation in the MV-LC networks using the MMC-based STATCOM is usually limited by the available semiconductor technology due to the voltage and current ratings, losses and switching frequency. These requirements can be dealt with using the EMMC-based STATCOM. Considering the distortion, because the equivalent switching frequency of the EMMC (with two parallel MMC) is as twice as that of the MMC, it is expected that the EMMC to cover a frequency bandwidth as twice as that of the MMC. Moreover, if the apparent powers of both the MMC and the EMMC are the same, then the switch ratings of the MMC have to be selected as twice as the switch ratings of the EMMC; additionally, the dc capacitance of each HBM in the MMC needs to be higher than that of the EMMC. Therefore, these advantages motivate the use of the EMMC as a STATCOM for MV-LC applications, in particular in the MV–LC uninterruptable industry such as electric traction systems.

VI. CONCLUSION

This paper proposes a novel type of high-power MMC-based STATCOM for a full compensation of unbalanced and distorted nonlinear load in the MV-LC networks under the presence of both the load and the source harmonics. This modular MMC-based STATCOM introduces a transformerless design, employing several isolated units composed of a number of cascaded HBM. Then, the EMMC-based STATCOM is developed by paralleling a number of MMC to achieve higher efficiency, higher reliability, lower weight and size, lower switching frequency and lower ratings for the switches. Various control strategies are suggested for both MMC and the EMMC in order to generate the reference currents for the compensator, followed by another strategy to get their corresponding reference voltages. Another controller is responsible for regulating all dc-link capacitor voltages at a predetermined level. Simulations and experiments were arranged for both the MMC and EMMC-based STATCOM. The practical work were performed on two 15-kVA modular MMC that can be presented as either MMC or EMMC. The control strategies were implemented on a DSP TMS320F2812. Simulations and experiments show proper operation of both proposals under unbalanced-distorted conditions.

ACKNOWLEDGMENT

The authors would like to thank the efforts made by the related officials of Power Quality and Reactive Power Control Laboratory, K. N. Toosi University of Technology, where the experimental works were performed.

REFERENCES

[1] P.-C. Tan, R. E. Morrison, and D. G. Holmes, "Voltage form factor control and reactive power compensation in a 25-kV electrified railway system using a shunt active filter based on voltage detection," *IEEE Trans. Ind. Appl.*, vol. 39, no. 2, pp. 575–581, Mar./Apr. 2003.

[2] M. T. Bina and M. D. Panahlou, "Design and installation of a 250 kVAr D-STATCOM for a distribution substation," *Elsevier: Electric Pow. Syst. Res.*, vol. 73, no. 3, pp. 383–391, Apr. 2005.

[3] F. Z. Peng and J. Wang, "A universal STATCOM with delta-connected cascade multilevel inverter," in *Proc. 35th Annu. IEEE Pow. Electron. Spec. Conf.*, Aachen, Gennany, Jun. 2004, pp. 3529–3533.

[4] R. E. Betz, T. Summerst, and T. Furney, "Using a cascaded H-bridge STATCOM for rebalancing unbalanced voltages," in *Proc. 7th Int. Conf. Pow. Electron.*, Daegu, Korea, Oct. 2007, pp. 1219–1224.

[5] F. Z. Peng, J. Wang, McKeever, and D. J. Adams, "A power line conditioner using cascade multilevel inverters for distribution systems," *IEEE Trans. Ind. Appl.*, vol. 34, no. 6, pp. 1293–1298, Nov./Dec. 1998.

[6] H. Akagi, S. Inoue, and T. Yoshii, "Control and performance of a transformerless cascade PWM STATCOM with star configuration," *IEEE Trans. Ind. Electron.*, vol. 43, no. 4, pp. 1041–1049, Jul./Aug. 2007.

[7] C. K. Lee, J. S K. Leung, S. Y R. Hui, and H. S. H. Chung, "Circuit-level comparison of STATCOM technologies," *IEEE Trans. Pow. Electron.*, vol. 18, no. 4, pp. 1084–1092, Jul. 2003.

[8] R. E. Betz, T. Summers, and T. Furney, "Symmetry compensation using an H-bridge multilevel STATCOM with zero sequence injection," in *Proc. Ind. Appl. Conf.*, Oct. 2006, pp. 1724–1731.

[9] H. M. Pirouz and M. T. Bina, "New transformerless STATCOM topology for compensating unbalanced medium-voltage loads," in *Proc. 13th Eur. Conf. Pow. Electron. Appl.*, Barcelona, Spain, Sep. 2009, pp. 1–9.

[10] R. Marquardt, "Stromrichters chaltungen mitverteilten Energiespeichern," German Patent DE 10 103 031, Jan. 24, 2001.

[11] S. Rohner, S. Bernet, M. Hiller, and R. Sommer, "Modulation, losses and semiconductor requirements of modular multilevel converters," *IEEE Trans. Ind. Electron.*, vol. 57, no. 99, pp. 2633–2642, Aug. 2009.

[12] J. Rodríguez, S. Bernet, B. Wu, J. O. Pontt, and S. Kouro, "Multilevel voltage-source-converter topologies for industrial medium-voltage drives," *IEEE Trans. Ind. Electron.*, vol. 54, no. 6, pp. 2930–2945, Dec. 2007.

[13] C. D. Schauder, "Advanced static var compensator control system," U.S. Patent 5 329 221, Jul. 12, 1994.

[14] M. T. Bina and A. K. S. Bhat, "Averaging technique for the modeling of STATCOM and active filters," *IEEE Trans. Pow. Electron.*, vol. 23, no. 2, pp. 723–734, Mar. 2008.

[15] M. Hagiwara and H. Akagi, "Control and experiment of pulse-width-modulated modular multilevel converters," *IEEE Trans. Pow. Electron.*, vol. 24, no. 7, pp. 1737–1746, Jul. 2009.

[16] H. Akagi, E. Watanabe, and M. Aredes, *Instantaneous Power Theory and Applications to Power Conditioning*. Hoboken, NJ: Wiley, 2007.

[17] L. Asiminoaei, E. Aeloiza, P. N. Enjeti, and F. Blaabjerg, "Shunt active-power-filter topology based on parallel interleaved inverters," *IEEE Trans. Ind. Electron.*, vol. 55, no. 3, pp. 1175–1189, Mar. 2008.
[18] J. Rodríguez, J. Lai, and F. Z. Peng, "Multilevel inverters: A survey of topologies, controls, and applications," *IEEE Trans. Ind. Electron.*, vol. 49, no. 4, pp. 724–738, Aug. 2002.
[19] Q. Song and W. Liu, "Control of a cascade STATCOM with star configuration under unbalanced conditions," *IEEE Trans. Pow. Electron.*, vol. 24, no. 1, pp. 45–58, Jan. 2009.
[20] R. Naderi and A. Rahmati, "Phase-shifted carrier PWM technique for general cascaded inverters," *IEEE Trans. Pow. Electron.*, vol. 23, no. 3, pp. 1257–1269, May 2008.

H. Mohammadi P. (S'08) was born in Mashhad, Iran, on December 28, 1980. He received the M.S. degree from the K. N. Toosi University of Technology, Tehran, Iran, in September 2005. He is currently working toward the Ph.D. degree (under supervision of Dr. M. Tavakoli Bina) at the Faculty of Electrical and Computer Engineering, K. N. Toosi University.

His research interests include design, modeling and control of high power electronics converters and their applications as FACTS controllers.

Mr. Pirouz is a student member of the Institute of Engineering and Technology.

M. Tavakoli Bina (S'98–M'01–SM'07) received the B.Sc. degree from the University of Tehran, Tehran, Iran, in 1988, the M.Sc. degree from the University of Ferdowsi, Mashhad, Iran, in 1991, and the Ph.D. degree from the Department of Electronics and Computer Engineering, University of Surrey, Guildford, U.K., in 2001, all in power electronics and power system utility applications.

From March 1992 to November 1997, he was a Lecturer at the K. N. Toosi University of Technology (KNTU), Tehran, working on power systems. Since September 2001, he has been with the Faculty of Electrical and Computer Engineering, KNTU, where he is currently an Associate Professor. His main research interests include power converters, modulation techniques, control and modeling of FACTS controllers, distribution systems, and power system control.